Soft Matter

Bending Behavior of CNT Fibers and their Scaling Laws

Journal:	*Soft Matter*
Manuscript ID	SM-ART-05-2018-001129.R1
Article Type:	Paper
Date Submitted by the Author:	23-Jul-2018
Complete List of Authors:	Adnan, Mohammed; Rice University, Chemical and Biomolecular Engineering Pinnick, Robert; Rice University, Chemical and Biomolecular Engineering Tang, Zhao; Rice University, Chemical and Biomolecular Engineering Taylor, Lauren; Rice University, Chemical and Biomolecular Engineering Pamulapati, Sushma Sri; Rice University, Chemical and Biomolecular Engineering Royer Carfagni, Gianni ; University of Parma, Department of Engineering and Architecture Pasquali, Matteo; Rice University, Chemical and Biomolecular Engineering

Journal Name

ARTICLE TYPE

Cite this: DOI: 10.1039/xxxxxxxxxx

Bending Behavior of CNT Fibers and their Scaling Laws†

Mohammed Adnan,*[a] Robert A Pinnick,*[a], Zhao Tang[a], Lauren W Taylor[a], Sushma Sri Pamulapati[a], Gianni Royer Carfagni [b§] and Matteo Pasquali[a‡]

Received Date
Accepted Date

DOI: 10.1039/xxxxxxxxxx

www.rsc.org/journalname

Carbon nanotube (CNT) fibers are a promising material for wearable electronics and biomedical applications due to their combined flexibility and electrical conductivity. To engineer the bending properties for such applications requires understanding how the bending stiffness of CNT fibers scales with CNT length and fiber diameter. We measure bending stiffness with a cantilever setup interpreted within Euler's elastica theory. We find that the bending stiffness scales with a power law of 1.9 for the fiber diameter and 1.6 for the CNT length. The diameter scaling exponent for fiber diameter agrees with results from earlier experiments and theory for microscopic CNT bundles. We develop a simple model which predicts the experimentally observed scaling exponents within statistical significance.

1 Introduction

Carbon nanotubes (CNTs) have exceptional physical properties, e.g., high tensile strength and electrical and thermal conductivities, at lower density and higher flexibility than classical materials.[1] Due to their flexibility, CNT fibers, threads, and yarns appear to be promising for applications in wearable electronics with intrinsic functionality, such as health monitoring, flexible antennas for wireless communications, flexible batteries, supercapacitors and photodetectors.[2–6] In addition, flexibility is critical for potential biomedical applications of single filament CNT fibers (diameter of the order of 10 μm) such as neural electrodes for deep brain stimulation for the treatment of neural diseases, replacement of damaged discrete neural bundles, or electrically-conductive cardiac sutures for the treatment of cardiac arrhythmia.[7–11] Therefore, it is important to understand the bending response of CNT fibers as a function of the characteristic parameters so that fibers can be tuned for these applications.

In order to understand prior work, it is useful to recall the classical theories used to describe the deformation of rods (or beams) under bending. The Euler Elastica (EE) can account for arbitrarily large displacements (such as in clock springs). It constitutively assumes that the bending moment depends linearly upon the local curvature *via* the bending stiffness κ, and that this is the only type of deformation. A simplification is Euler-Bernoulli Theory (EBT), which approximates the curvature by the second derivative of the transversal displacement of the rod - a hypothesis that holds only for small rotations (linear deformation). When the material is an elastic homogeneous isotropic monolith, $\kappa = EI$, where E is the Young's modulus, and I the moment of inertia of the cross section around the bending axis (the principal axis of inertia). Therefore, the bending stiffness scales with the fourth power of the beam's diameter. Both EE and EBT assume "pure bending states", i.e., they exclude the effects of shear deformations. The Timoshenko beam theory (TBT) distinguishes shear from bending deformations. With the same hypothesis of geometric linearity, the TBT tends to the EBT for high aspect ratio (L/D), where L is the length of the beam and D the diameter of its cross section. Moreover, TBT predicts that the bending stiffness of a beam scales essentially with the second power of diameter only when the beam has low aspect ratio, and the shear modulus is much lower than the elastic modulus.

While no prior work specifically considers the bending stiffness of macroscopic CNT fibers, the bending stiffness of microscopic bundles of CNTs has been extensively studied both theoretically and experimentally.[12–18] Salvetat et al.[12] performed experiments on the deflection of microscopic CNT bundles with varying length and diameter. These deflections were analyzed with TBT to correlate the measured displacements to the beam stiffness; experiments showed that the CNT bundle bending stiffness scaled with bundle diameter with a power law lower than four, even though the experiments were conducted in the regime of slender beams, where TBT should approach EBT. Salvetat et al. attributed this unusual scaling it to an unusually low, nonphysical value of the shear modulus, and later corroborated this interpretation with ex-

[a] *Rice University, 6100 Main St. MS-369, Houston, TX, USA.*
[b] *University of Parma, Parco Area delle Scienze 181/A, I-43100, Parma, Italy.*
† Electronic Supplementary Information (ESI) available: CNT fiber characterization and bending stiffness data. See DOI: 10.1039/b000000x/
‡Corresponding Author - Tel: +1-713-348-5830; E-mail: mp@rice.edu
§Corresponding Author - Tel: +39 0521 906606; E-mail: gianni.royer@unipr.it

periments on partially crosslinked fibers.[14–16] Moreover, Salvetat et al. introduced a diameter-dependent shear modulus, but this is not consistent with the classical TBT model.

Yakobson and Couchman[19] argued that the bending stiffness of CNT bundles should fall between two limiting cases. On the lower end, the CNTs act as independent rods, and the bending stiffness is the product of the number of CNTs in the bundle and the bending stiffness of the individual CNTs. This means the bending stiffness will scale with the fiber diameter to the second power. On the upper end, the CNTs form a coherent bundle where the rods cannot slip past one another, so the bending stiffness scales as a power law of 4.[19] These two limiting cases are well known and, in the language of laminated-structure mechanics, are usually referred to as the "layered" and the "monolithic" limit, respectively.[20]

Pipes et al.[17,18] derived a model for the bending behavior of CNT bundles considered as laminated structures with partial shear coupling of the constituent layers, i.e., an intermediate condition between the layered and the monolithic limits. In their model, the CNT bundles are treated as a hexagonal array of discrete rod-like elements forming laminate layers, instead of a homogeneous cylindrical body. In addition to bending and elongating, the layers transfer stress via relative shearing, according to an experimentally determined "shear transfer efficiency parameter", which is uncorrelated with the fiber diameter.[17,18] This simple approach has been widely proposed in the past to interpret the response of laminated structures; its difference with TBT consists of the fact that the shear interaction among the CNT layers is uncorrelated with the Young's modulus of the CNTs. However, it suffers the particular drawback that the "shear transfer efficiency parameter" should depend upon the length of the fiber and the type of loading (size- and load-dependence), but this correlation does not seem to have been sufficiently investigated for the case of CNTs.[21]

A more refined model was proposed by Bathe et al.[22] who explicitly considered the micromechanics of sliding rods. In their model, the bundle is assumed to be composed of rods with monodisperse length. The bending curvature results in the bending of the constituent rods, as well as in an internal mismatch (relative sliding) between the lengths of the contact regions between adjacent rods. This mismatch gives rise to intramolecular extension/compression and intermolecular shear that can be explicitly accounted for provided that the associated energy functional is known. Negligible coupling between the rods recovers the layered limit. For perfect shear coupling, the path-length change results in an extension/compression of the rods and the bending stiffness behaves according to the monolithic limit. Models of this kind are classical in the mechanics of layered sandwich structures.[23] Compared to the simple approach by Pipes et al., Bathe et al. explicitly consider the geometric properties of the constituents rods, as well as the boundary and loading conditions. However, in this model, the length of the constituent rods is assumed to be equal to the length of the fibers.

The experimental data and theoretical models of microscopic bundles of CNTs differ from other natural and synthetic textile fibers. The stiffness of CNT bundles does not follow the power law of four expected by EBT; conversely, short segments of monofilament textile fibers are reasonably described with EBT.[24–28] Vilatela and Windle have argued that CNT fibers are not characteristically similar to monofilament textile fibers but instead to multifilament yarns.[29,30] Classically, monofilament textile fibers exhibit a monolithic response to bending, whereas the behavior of yarns depends on the shear coupling among the individual filaments in the yarn.[28,31,32] Therefore, major attention should be paid to the proper modeling of the compliance associated with intermolecular forces that keep together the constituent CNT rods. Moreover, geometrical nonlinearities are important for flexible, yarn-like filaments and should be captured appropriately by using at least the EE model.

An important shortcoming of existing literature models is that they do not explicitly consider the length of the constituent CNTs, which is always much smaller than the length of the fiber. Here, we measure the bending deformation of macroscopic CNT fibers as a function of fiber diameter and CNT length. We model the deformation shapes with EE, as EBT and TBT fail to capture the relevant geometric nonlinearities. We provide an elementary model for the interpretation of the measured dependence of the bending stiffness upon fiber diameter and CNT length.

2 Experimental

2.1 Specimen Preparation

2.1.1 CNT Preparation

We used CNTs (EC1.5S synthesized by Meijo Nano Carbon Company Ltd.) with a diameter of ∼1.5 nm.[33] The raw CNTs are a mixture of single-walled CNTs and double-walled CNTs with impurities of amorphous carbon and iron oxide. Removal of the impurities was carried out by slightly modified literature protocols.[34,35] Amorphous carbon was removed via exposure to 80% N_2 and 20% O_2 flowing at 100 sccm in a $2^1/_2$" tube furnace (Mellen NACCI™) at 480 °C (Table 1). To remove the iron oxide catalyst, the purified CNT samples were washed in 37% HCl (EMD Millipore) for more than 12 hours. The acid wash step was repeated until no color change was observed in the acid, which indicates negligible residual iron dissolution. The purified CNTs were washed with deionized water until a neutral pH was obtained and subsequently freeze-dried (Millrock Bench Top Manifold Freezer Dryer BT48) for 24 hours to remove the water.

At elevated temperatures, thermal oxidation shortens CNTs due to the higher reactivity of the tube ends.[36] To shorten the CNTs, the purified CNTs were heated to a target temperature in a $2\ ^1/_2$" tube furnace under pure N_2 flowing at 100 sccm. The CNTs were exposed to pure O_2 for a specific duration and were then cooled to ambient temperature under pure N_2 flowing at 100 sccm. Oxidation temperatures and duration are shown in Table 1. As thermal oxidation may generate amorphous carbon and functionalize the CNTs, Raman spectroscopy of the original and shortened CNTs was measured on a Renishaw Raman microscope. This indicated negligible functionalization of the CNTs.

The length of the original and shortened CNTs was determined from the aspect ratio (ratio of the length to diameter). The aspect ratio was measured from extensional rheometry with the exper-

Table 1 CNT preparation conditions and resulting aspect ratios. The data are reported with ± 1 standard deviation.

Purification Time	Oxidation Time	Oxidation Temperature	Aspect Ratio
hrs	mins	^{o}C	L/D
3.5	12	675	1471 ± 90
20	5	525	2780 ± 110
11	0	-	4185 ± 159

imental setup and procedure of Tsentalovich et al.[33] The procedure was slightly altered with a stretching speed of 10 mm/s instead of 25 mm/s. The aspect ratio measurements were performed in triplicate.

2.1.2 Fiber Preparation

CNT fibers were prepared via the solution spinning process of Behabtu et al.[37] In this process, CNTs were dissolved into chlorosulfonic acid (Sigma Aldrich 99%) at a concentration of 2 wt. %. The solutions were speed-mixed for 60 to 120 minutes at 2350 rpm in a FlackTex DAC 600 SpeedMixer™. The mixed solutions were extruded through a spinneret at a linear velocity of approximately 2 m/min into an acetone (Sigma Aldrich 99.9%) coagulant bath and drawn at the maximum stable draw ratio. Subsequently, the CNT fibers were washed in water and dried in an oven at 115 °C. Fibers were prepared varying the spinneret diameter (100 μm, 125 μm, and 150 μm) and the CNT lengths (2.21 μm, 4.17 μm, 6.28 μm). The spinneret diameter was varied holding the CNT length constant at 6.28 μm and the CNT length was varied holding the spinneret diameter constant at 150 μm.

To remove any deformation history in the CNT fibers, fibers of approximately 25 cm in length were hung vertically with a mass of 1.3 g in an oven at 115 °C for at least 4 hours. This annealing under moderate tension allowed the fibers to straighten and relax any locked-in bending stresses. The fibers were then allowed to hang under tension for at least 6 hours in a glove box to unwind any twisting that may have occurred. Afterwards, the straight fibers were placed on a Teflon block and cut to length with the tip of a sharp razor blade.

2.1.3 Fiber Characterization

An optical microscope (Zeiss AxioPlan 2) was used to measure diameters of random sections of a fiber. Numerous measurements were taken to ensure good representation of the diameter. The length of the fiber was measured using a millimeter ruler, and an average of 3 measurements were made to record the mass of the fiber using a microbalance. Diameters and linear densities are reported in the ESI.†

High-resolution scanning electron microscopy (Helios NanoLab G3) was used with a focused gallium ion beam at a current of 65 nA and voltage of 30 kV to cut the fibers and image the fiber cross section. Representative images are in the ESI.†

The Young's moduli of the fibers were determined from their stress-strain responses as measured by ARES G2 rheometer (TA Instruments). Tensile testing was performed on 3 cm long fibers at a rate of 0.01 mm/s. The tensile tests were performed in triplicate. Tensile test results are reported in the ESI.†

Despite the high degree of CNT axial alignment and packing in the fibers[37,38], the measured Young modulus E_M ranged between 66 and 231 GPa, well below the theoretical modulus of CNTs $E_T \approx$ 730 GPa,* indicating incomplete coupling between the CNTs in the fibers.[39]

2.2 Measuring Bending Stiffness

2.2.1 Cantilever Setup

A series of cantilever experiments were performed to measure the bending modulus of CNT fibers using a setup similar to Clapp et al.[40] The free end of the fiber specimen was allowed to hang under self-weight as a cantilever at various lengths while the other end was clamped. Fibers tend to collapse (by kinking) for long lengths of cantilever. The typical deformation is shown in Figure 1. The fiber was pulled backwards, thus decreasing the cantilever length until the deformation was not appreciable: more than 15 snapshots of the cantilever were taken for each fiber as the cantilever length decreased. Disturbances from air currents swaying the fiber were minimized by enclosing the set up within a glovebox. A point-and-shoot camera mounted on a tripod was used to take images of the cantilever against a white background containing scale-bars. To obtain the cantilever profiles, the images were processed using the algorithm of Brangwynne et al. in Matlab.[41]

2.2.2 Calculation of Bending Stiffness

Figure 2 shows that the profiles of the CNT fiber cantilevers deviate from EBT and TBT indicating either geometric and/or constitutive non-linearities. Assuming the constitutive non-linearities are negligible, then the geometric non-linearities can be described with EE, whose governing equation reads

$$\frac{d^2\psi}{dS^2} = -\frac{wS}{\kappa}\cos\psi \tag{1}$$

where, as represented in Figure 3, $\psi(S)$ is the slope of the cantilever, κ is the bending stiffness, w is the weight of the cantilever per unit-length (supposed uniform), and S is the curvilinear coordinate parametrized by arc length of the cantilever, with the free end as the origin. The slope of the cantilever is related to the abscissa x, associated with its horizontal projection, by

$$x(S) = \int_0^S \cos\psi(\xi)\, d\xi\,. \tag{2}$$

Unfortunately, Equation (1) cannot be solved analytically for a horizontal cantilever with a uniform vertical force for all conditions. For a restricted parameter space, Scarpello showed that (1) can be expressed in terms of Lauricella hypergeometric functions.[43] Approximate solutions have been developed based on power series[42,44–46], series of Chebyshev polynomials[47], perturbation methods[48], and homotropy analysis method.[49] For this analysis, we use the power series approximation given in Equation (5.30) from Frisch-Fay[42], which provides the function $y(S)$

* The theoretical modulus of CNTs is typically reported on the basis of the cross-sectional area of the CNT wall with $E_T \approx 1$ TPa. The reported value in the text above is based on the cross-sectional area of a hexagonal bundle of CNTs.

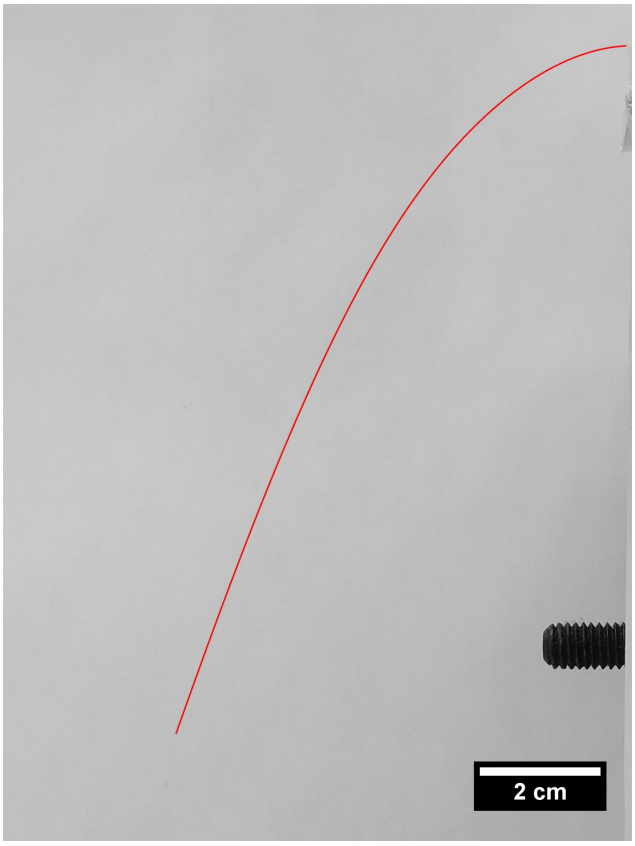

Fig. 1 Image of cantilever setup with overlay of cantilever profile (processed in Matlab) for a representative sample of CNT fiber spun from a 150 μm spinneret.

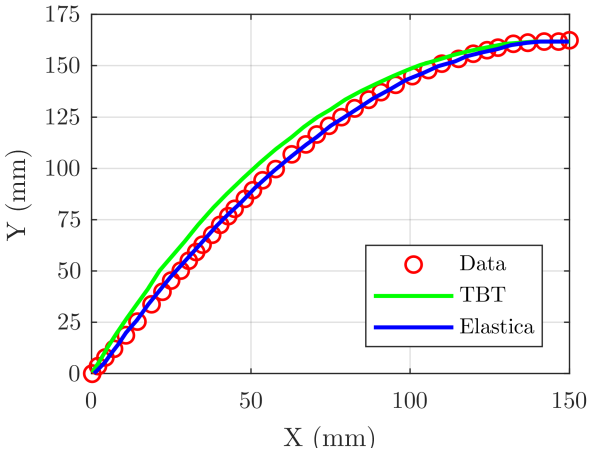

Fig. 2 TBT and EE fits to a representative cantilever profile for CNT fiber with CNT length of 6.28 μm.

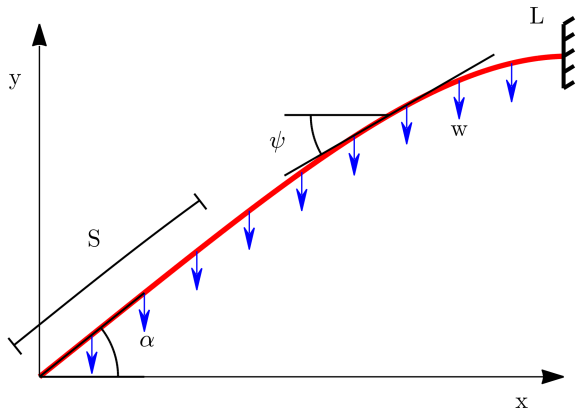

Fig. 3 Profile of horizontal cantilever bending under a uniform vertical load of the fiber's weight. Adapted from Frisch-Fay.[42]

associated with the cantilever profile in the form

$$
\begin{aligned}
y &= \sum_{i=0}^{3} c_i \left(\frac{w}{\kappa}\right)^i \\
c_0 &= S \sin\alpha \\
c_1 &= -S^4 \frac{\cos^2\alpha}{24} \\
c_2 &= -S^7 \frac{\sin\alpha\cos^2\alpha}{360} \\
c_3 &= S^{10}\cos^2\alpha\left(\frac{\cos^2\alpha}{10368} - \frac{13}{129600}\sin^2\alpha\right)
\end{aligned}
\tag{3}
$$

where α is the bending angle of the cantilever at the free end (Figure 3). Assuming this model, we can measure the bending stiffness in Equation (1) by fitting the displacement at the free end.

Figure 2 shows that EE captures the cantilever profile much better than TBT. We also note that the best fit for the TBT is associated with a shear modulus $G \simeq 30$ TPa, which is unrealistic. To verify the assumption of negligible constitutive non-linearities, the effective bending stiffness κ was determined for each fiber using different cantilever lengths (2 cm $\leq L \leq$ 25 cm), providing bending moments of different amplitude. As shown in Figure 4, within this range of cantilever lengths, the measured effective bending stiffness fluctuates around a mean value independent of the cantilevered length, confirming that EE captures accurately the fiber behavior (the scatter in the measured data is associated with variation of fiber diameter and circularity along their length, as discussed further below). All values of the bending stiffness recorded hereafter were determined by best fitting the cantilever deflection with EE.

2.2.3 Statistical Analysis

Because the fiber cross section is not perfectly round and uniform along the fiber length and there are inherent experimental errors

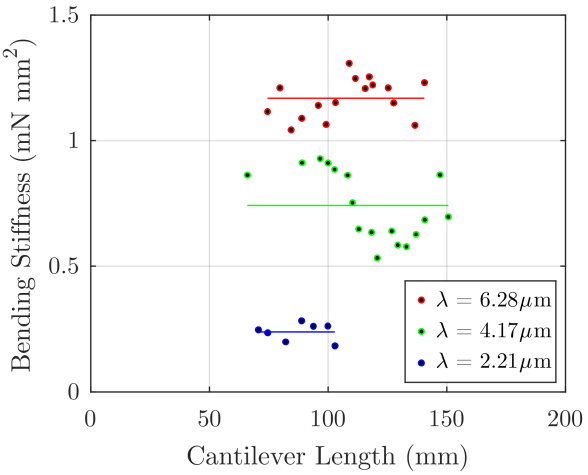

Fig. 4 Bending stiffness from EE varying the cantilever length for representative fiber segments for CNT fibers spun from spinneret diameter of 150 μm and with CNT length of 2.21 μm (blue), 4.17 μm (green), 6.28 μm (red).

in the measurements of fiber cantilevered length and deflection, together with uncertainties in the measurement of CNT length, we performed a statistical analysis of our measurements as to assess their statistical meaningfulness. The statistical distribution of the power law exponents was determined by bootstrap analysis[50], except that we assumed a Gaussian CNT length distribution because of the small number of length measurement experiments (n=3 for each CNT sample).

The power law for bending stiffness with fiber diameter was determined by case resampling and least squares regression. The regression was performed on sample sets of the bending stiffness data sampled with replacement and connected to an estimate of the average fiber diameter from the different spinneret sizes. The estimate for the average fiber diameter was taken as the average of a sample set of the fiber diameter data sampled with replacement at each spinneret size. The power law for CNT length was determined by case resampling and least squares regression on sample sets of bending stiffness sampled with replacement; each set was then connected to an estimate of the CNT length.

3 Results and Discussion

3.1 Experimental Results

Bending stiffness of CNT fibers as a function of fiber diameter and CNT length were determined with the method outlined above. The bending stiffness κ from EE determined by varying CNT length is given in Table 2 and by varying fiber diameter is given in Table 3. For the sake of comparison, in the same tables the measured values of bending stiffness are compared with the quantity $(E_T I)$, i.e., the product of the theoretical Young's tensile modulus $E_T \approx 730$ GPa and the cross-sectional moment of inertia.

Although the assumption (underlying EBT and TBT) that the fiber is made of a monolithic isotropic elastic material does not hold for CNT fibers, the framework is commonly used for natural and polymeric fibers[24–28] and has been applied to bundles of CNTs.[12,14–16] As such, these theories provide a reference point

Table 2 Measured bending stiffness κ for CNT fibers varying CNT length at a constant spinneret diameter of 150 μm. Comparison with the product $(E_T I)$ of the theoretical Young's tensile modulus and the cross-sectional moment of inertia. The data are reported with $\pm$ 1 standard deviation.

CNT Length $\langle\lambda\rangle$	Fiber Diameter	Bending Stiffness κ	$E_T I$
μm	μm	mN·mm^2	mN·mm^2
2.21 $\pm$ 0.24	22.4 $\pm$ 0.8	0.22 $\pm$ 0.09	8.98 $\pm$ 0.34
4.17 $\pm$ 0.17	22.1 $\pm$ 0.6	0.74 $\pm$ 0.14	8.49 $\pm$ 0.21
6.28 $\pm$ 0.14	22.0 $\pm$ 1.8	1.08 $\pm$ 0.18	8.31 $\pm$ 0.70

Table 3 Measured bending stiffness κ for CNT fibers varying fiber diameter at a constant CNT length of 6.28 μm. Comparison with the product $(E_T I)$ of the theoretical Young's tensile modulus and the cross-sectional moment of inertia. The data are reported with $\pm$ 1 standard deviation.

CNT Length $\langle\lambda\rangle$	Fiber Diameter	Bending Stiffness κ	$E_T I$
μm	μm	mN·mm^2	mN·mm^2
6.28 $\pm$ 0.24	12.4 $\pm$ 0.7	0.33 $\pm$ 0.06	0.86 $\pm$ 0.05
6.28 $\pm$ 0.24	17.7 $\pm$ 2.9	0.79 $\pm$ 0.15	3.53 $\pm$ 0.57
6.28 $\pm$ 0.24	22.0 $\pm$ 1.8	1.08 $\pm$ 0.17	8.31 $\pm$ 0.70

for comparison. Implicitly, these theories assume that the bending stiffness is independent of CNT length and should scale with the fourth power of the fiber diameter. Figure 5 shows that the bending stiffness calculated from EE analysis scales with the 1.57 power with CNT length and the scaling exponent of 1.94 with fiber diameter. The uncertainty in the scaling exponents is shown in Figure 5(b) and 5(d). The nonzero scaling exponent for CNT length and the weak scaling exponent for fiber diameter indicate that the CNT fiber does not behave as a monolithic isotropic material, i.e., there is a relative elastic sliding deformation between the CNTs that reduces the bending stiffness, and that such sliding is reduced for longer CNTs—consistent with the observation that the measured tensile modulus E_M is much lower than the theoretical one E_T and increases with CNT length. Notably, the weak power-law exponent cannot be attributed to the potential effects of shearing in a monolith because the TBT model does not predict accurately the cantilever profile (Figure 2).

3.2 An Elementary Model

Following the approach of Bathe et al., an elementary model is now presented that takes into account the aspect ratio of the constituent CNTs.[22]

Suppose that in the undistorted state, the fiber is straight and composed of a set of parallel CNTs. As shown in Figure 6*a*, we introduce a reference system (x,y,z) with the y axis parallel to the fiber length and centroidal with respect to the fiber cross section. Then, the fiber is bent in the $y-z$ plane such that the centroidal fibers, $z=0$, form a constant radius of curvature ρ, considered positive if the center of curvature is directed towards the positive direction of z. Neglecting the transversal strain, the radius of curvature for a given CNT is approximately constant and de-

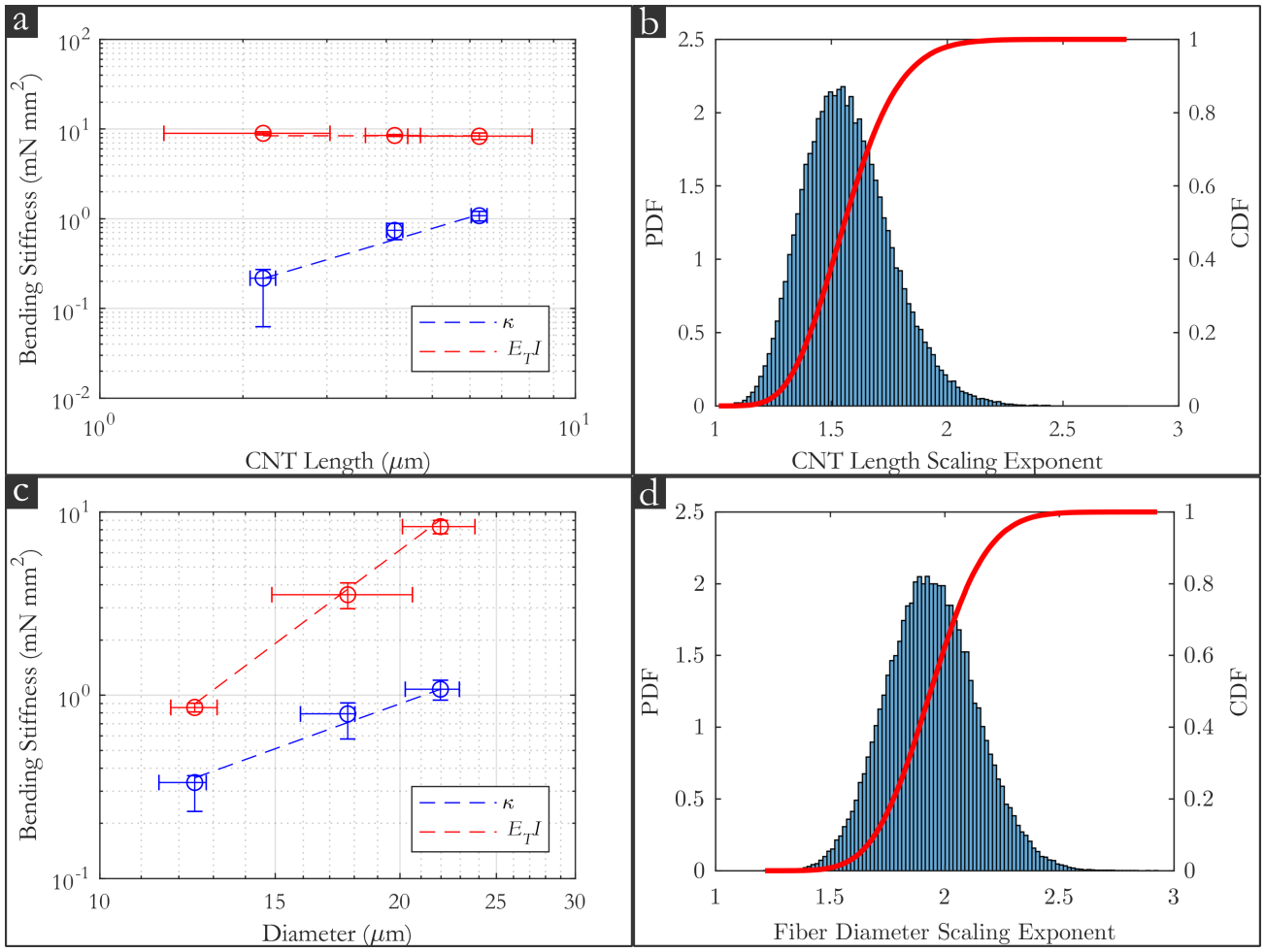

Fig. 5 Power law fits for E_TI and the bending stiffness κ from EE: (a) dependence on CNT length; (b) PDF and CDF of the scaling exponent between CNT length and bending stiffness; (c) dependence on fiber diameter; (d) PDF and CDF of the scaling exponent between fiber diameter and bending stiffness. The ranges in (a) and (c) are the 68% confidence interval, which is 1 standard deviation for a Gaussian distribution.

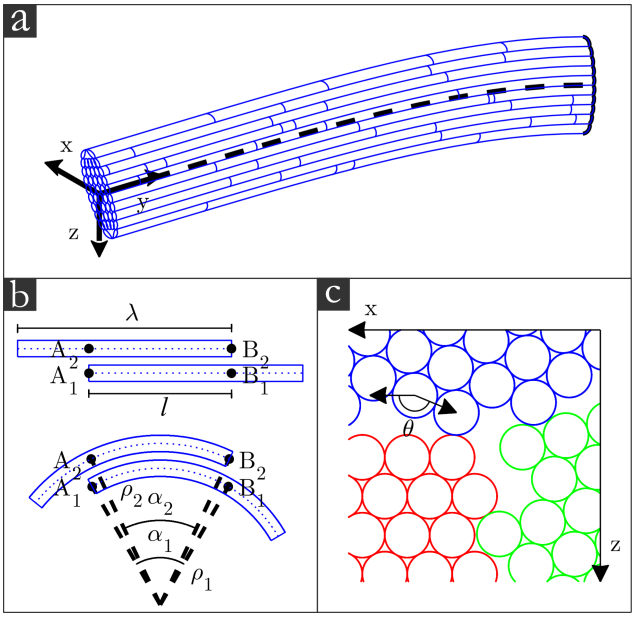

Fig. 6 (a) Local coordinate system for CNT fiber. (b) Undeformed and deformed conformation of a pair of CNTs before and after bending as shown in the YZ plane of the fiber. (c) Conceptual representation of the polycrystalline structure and the orientation angle θ, for a pair of CNTs shown in the XZ plane cross section of the fiber. The colors (red, green, and blue) indicate different crystalline domains within the fiber.

pends upon its z coordinate. We assume that each CNT has a proper bending stiffness associated with the parameter κ_b, so that its bending energy can be expressed in the form

$$\varepsilon_b = \frac{1}{2}\frac{\kappa_b \lambda}{(\rho - z)^2} \tag{4}$$

where λ is its length and $(\rho - z)$ is its radius of curvature, which depends upon the position z. Due to the high density of solution spun fibers, the density of CNTs can be reasonably approximated as being uniform in a considered segment of fiber.[37] If N is the total number of CNTs in a segment of fiber of volume V, averaging over both the length distribution and the cross section gives an expression for the average bending energy of the single CNT $\langle \varepsilon_b \rangle$ of

$$\langle \varepsilon_b \rangle = \frac{1}{N}\iint_A \frac{1}{2}\frac{\kappa_b \langle \lambda \rangle}{(\rho - z)^2} dx\, dz \int_0^L dy \frac{N}{V}. \tag{5}$$

In general, the radius of curvature of the bent fiber is of the order of a few centimeters, whereas the diameter of the fiber is of few tenths of a millimeter. Therefore, since $\rho \gg z$, one has that $\rho - z \simeq \rho$, so that the bending free energy per volume is approximately given by

$$\frac{\Theta_b}{V} \simeq \frac{N}{V}\frac{1}{2}\frac{\kappa_b \langle \lambda \rangle}{\rho^2}. \tag{6}$$

We also assume that there is a certain degree of connection of the constituent CNTs along their lateral surface, which constrains their relative sliding, due to inter-CNT shear forces. The intermolecular shear energies depend upon the mismatch between the lengths of the contact regions of adjacent CNTs induced by their relative sliding. Due to the high degree of alignment of CNTs along the fiber axis, the CNTs can be assumed to be approximately parallel.[37] As such, let l denote the overlap length of the CNTs in the undeformed configuration (Figure 6*b*). Consider two adjacent CNTs (denoted by the labels 1 and 2) and let the corresponding radii of curvature be ρ_1 and ρ_2 respectively. The difference in radius of curvature is related to the angle of the rods relative to the bending plane and, with the notation shown in Figure 6*c*, reads

$$\rho_2 - \rho_1 = d \sin\theta \tag{7}$$

where θ is the polar angle between the line passing through the centroid of the CNTs in lateral contact and the x axis, while d is the diameter of the CNT.

For the deformation of two parallel overlapping CNTs, the dominate energy scale is a function of the length of the rods due to the competition between the Young's modulus of CNTs and the shear modulus between rods. At short lengths, there is a mild connection among the fibers, so that the CNTs cannot undergo noteworthy axial strain (they behave as being inextensible): the shear energy scale dominates, and the rods slide under a deformation. At long lengths, the resultant of the shear contact forces is sufficient to equilibrate the shear induced by bending, so that the rods behave as if they do not slide past one another. Thus, the tensile energy dominates, and the rods stretch under a deformation.[51] Based on tensile strength tests for a variety of fibers, CNTs with lengths on the order of 1 to 10 μm are still in the short rod regime where shear energy dominates.[38] As a first approximation, the shear energy can be estimated by a pair of overlapping and neighboring CNTs and the number of neighboring pairs of CNTs. The intermolecular interactions drop rapidly so non-neighboring CNTs should have minimal contribution to the energy of the system.

To estimate this contribution in the deformed configuration, let α_1 and α_2 denote the angle spanned by the length l for the radius of curvature ρ_1 and ρ_2, respectively (Figure 6*b*). Due to the assumed axial inextensibility of the rods, one has $\alpha_1\rho_1 = \alpha_2\rho_2 = l$. Thus, the curvature-induced mismatch, δl, between the lengths of the contact regions reads

$$\begin{aligned}\delta l &= \alpha_1\left(\rho_1 + \frac{1}{2}d\sin\theta\right) - \alpha_2\left(\rho_2 - \frac{1}{2}d\sin\theta\right)\\ &= \frac{1}{2}\left(\frac{1}{\rho_1} + \frac{1}{\rho_2}\right) l\, d\, \sin\theta\\ &\simeq l\frac{d\sin\theta}{\rho}\end{aligned} \tag{8}$$

where we have made the approximation $\rho_1 \simeq \rho_2 \simeq \rho$.

For the shear energy, we assume a linear elastic potential in the limit of small deformations. Such linear relationship is a first order approximation of the periodic corrugation energy predicted by full atom simulations of CNTs in the quasi-static limit interacting via van der Waals forces.[52] Thus, the associated energy from shear between two CNTs is given by

$$\varepsilon_s = \frac{k_s l(\delta l)^2}{2} = \frac{k_s d^2 \sin^2\theta l^3}{2\rho^2}. \quad (9)$$

where k_s is a spring constant for the shear overlap. This constant collapses all sources of shear interaction among the constituent CNTs into a single parameter model. As the fiber can be thought of as a polycrystalline structure with the a priori assumption of uniform angular distribution, the ensemble average of the shear energy over the orientation and lengths is

$$\langle \varepsilon_s \rangle = \frac{k_s d^2 \langle l^3 \rangle}{4\rho^2}. \quad (10)$$

For the hexagonal arrangement as shown in Figure 6*c*, this calculation can be easily verified because for each rod there are 6 neighbors to take into account, 2 of which with $\theta = 0$ and the remaining 4 with $\sin^2\theta = 3/4$ ($\theta = \pm\pi/3$).

Assuming a symmetric and narrow overlap length distribution, the overlap distribution function should be symmetric. Thus, the third moment of the overlap length can be related to the first moment through a relationship of the form

$$\frac{\langle l^3 \rangle}{\langle l \rangle^3} = 1 - \eta \frac{\sigma^2}{\langle l \rangle^2} \quad (11)$$

where σ is the standard deviation of the overlap length distribution and η is a constant that depends upon the type of statistical distribution. For long CNTs, the latter term is negligible, and the ratio is approximately 1. The first moment of the overlap length is roughly proportional to half the average length of the CNTs. Therefore, the average shear energy per pair of CNTs is

$$\langle \varepsilon_s \rangle \simeq \frac{k_s d^2 \langle \lambda \rangle^3}{32\rho^2}. \quad (12)$$

As stated earlier, the total energy from shear of CNTs in a segment of fiber is approximately the product of the number of nearest neighboring rods and the average shear energy per pair of overlapping rods. Hence,

$$\Theta_s \simeq \frac{m}{2} N \langle \varepsilon_s \rangle \quad (13)$$

where m is the number of nearest neighbors and the factor $^1/_2$ is included to prevent double counting of nearest neighbor pairs.

The number of nearest neighbors is highly dependent on the fiber structure. A hexagonal lattice is the maximum dense packing structure for parallel rods. In this structure, the number of nearest neighbors is 12. As a comparison point for a square lattice, the number of nearest neighbors is 8. For lower density structures (e.g. hexatic phase), the number of nearest neighbors has a wide range, but the ensemble average number of nearest neighbors should decrease with decreasing fiber density. In addition, edge effects will decrease the number of nearest neighbors. However, for a fiber with a high volume to surface area ratio such as a circular fiber with a fiber diameter much larger than the diameter of the rod, edge effects should be negligible.

While the number of rods in a fiber segment is a function of the structure, it can just be incorporated in the volume fraction of rods, ϕ. Thus, the number of rods is

$$N = \phi \frac{4V}{\pi d^2 \langle \lambda \rangle}. \quad (14)$$

Combining Equations (6), (12), (13) and (14), the total energy per volume of fiber is

$$\frac{\Theta}{V} \simeq \frac{\phi}{16\pi\rho^2} \left(m k_s \langle \lambda \rangle^2 + 32 \frac{\kappa_b}{d^2} \right). \quad (15)$$

From this expression, one finds that the effective the bending stiffness is

$$\kappa_e \simeq \frac{A\phi}{8\pi} \left(m k_s \langle \lambda \rangle^2 + 32 \frac{\kappa_b}{d^2} \right) \quad (16)$$

where A is the cross-sectional area of the fiber.

When the shear bonding of the fiber is strong, the fiber is reasonably approximated by a monolith, for which the TBT or the EBT represent reasonable models. However, in this case, the tension/compression energy of the individual CNTs cannot be neglected as assumed for the elementary model. In other words, the expression (16) is valid only in a short CNT length regime where shear sliding among the fibers is high enough that the axial elongation of the constituent CNTs can be considered a second order effect. Moreover, as shown in Figure 6(b), the model assumes that the centers of two overlapping lengths, l, do not slide relative to one another. This implies that the shear contact stress is antisymmetric with respect to the center itself. In a more sophisticated approach, one might take into account a more general kinematics, but at the expenses of the simplicity of the model.

The bending stiffness is experimentally observed to scale to the fiber diameter with a power law exponent of 1.94, which agrees with this model despite its simplicity. As the moment of inertia is proportional to the fiber diameter to the power of 4, the measured stiffness would be equal to EI only provided that E decreased with a power law of -2 of the fiber diameter. However, this does not agree with experimental observations on tensile tests. As for the CNT length, the bending stiffness experimentally scales with a power law exponent of 1.57. This power law may be interpreted with Equation (16); the part associated with shear energy scales with CNT length to a power law of 2, while the bending energy of individual CNTs is independent of CNT length (power law with exponent 0). For very short CNT lengths, the bending energy of the individual CNTs is dominant and bending stiffness is independent of CNT length. For short CNT lengths, the energetic contribution from shear sliding increases and the power law exponent will approach 2. For an intermediate range of CNTs lengths, these energies will be on comparable scales and the power law exponent will take a value between 0 and 2. While not addressed in our simplified model, the fiber bending stiffness should become independent of CNT length in the limit of long CNT length. This implies another transitional regime (not captured by the simplified model) where the scaling exponent will transition from a power law of 2 to a power law of 0. The scaling exponent of 1.57 indicates that, in our fibers, the CNTs may be in a length range corresponding to a transition between scaling regimes.

The elementary model is based on an idealization of a real CNT fiber. Of course, imperfections in the fiber such as poor packing

and misalignment might alter the bending deformation mechanisms. However, fibers produced by the solution spinning technique have high alignment based on typical FWHM by XRD[37,38] and are well packed with small voids on the range of 100 nm as shown in the ESI.†Because of the dense packing, high alignment, and the good agreement of the model to experimental data, we believe that alternative deformation mechanisms do not play a dominant role in the bending stiffness of the CNT fiber.

4 Conclusions

A simple cantilever testing setup has been proposed for indirectly measuring the bending stiffness of macroscopic CNT fibers, without introducing mechanical kinking. To account for geometric non-linearities, the profiles were interpreted with EE. The bending stiffness was experimentally determined to scale with a power law of 1.57 for the length of the constituent CNTs and a power law of 1.94 for the fiber diameter. This is quite different from the expectation from monolithic elastic materials, where the bending stiffness should depend upon the moment of inertia of the fiber cross section. The diameter dependence is consistent with earlier experiments on microscopic CNT bundles as well as earlier models based on lateral friction.[19,53] While the fiber diameter scaling law may agree with the prediction from TBT in the limit of small shear modulus, this model fails to represent the measured deformation profile of the fiber cantilever.

An elementary model has been proposed to describe the bending response of the fiber as a laminate structure, which accounts for the longitudinal sliding of the constituent CNTs. This predicts a scaling exponent of the bending stiffness between 0 and 2 for CNT length and a scaling exponent of 2 for fiber diameter. This is in good agreement with the experimental finding, taking into account the simplicity of the model. Finally, this study suggests that the bending stiffness of CNT fibers is essentially governed by the relative sliding of the constituent CNTs along the bending axis. As the elementary model does not explicitly depend on the chemical structure of the CNT, the bending stiffness behavior of CNT fibers should be analogous to other highly aligned polymeric fibers such as aramid or graphene fibers.[54–56] This would be an interesting area for additional study.

Conflict of interest

There are no conflicts to declare.

Acknowledgments

Funding was provided by the Air Force Office of Scientific Research (AFOSR) grants FA9550-09-1-0590 and FA9550-15-1-0370 and the Welch Foundation grant C-1668. M.A. was partially supported by a Ph.D. scholarship from Abu Dhabi National Oil Company (ADNOC). L.W.T. was supported by a Ph.D. scholarship from NDSEG.

References

1 *Carbon Nanotubes: Synthesis, Structure, Properties, and Applications*, ed. M. Dresselhaus, G. Dresselhaus and A. P, Springer-Verlag, Berlin Heidelberg, 2001.

2 A. Dalton, S. Collins, E. Munoz, J. Razal, V. Ebron, J. Ferraris, J. Coleman, B. Kim and R. Baughman, *Nature*, 2003, **423**, 703.

3 C.-F. Sun, H. Zhu, E. Baker III, M. Okada, J. Wan, A. Ghemes, Y. Inoue, H. Liangbing and Y. Wang, *Nano Energy*, 2013, **2**, 987–994.

4 X. Wang, K. Jiang and G. Shen, *Materials Today*, 2015, **18**, 265–272.

5 E. A. Bengio, D. Senic, L. W. Taylor, D. E. Tsentalovich, P. Chen, C. L. Holloway, A. Babakhani, C. J. Long, D. R. Novotny, J. C. Booth, N. D. Orloff and M. Pasquali, *Applied Physics Letters*, 2017, **111**, 163109.

6 A. Zubair, X. Wang, F. Mirri, D. E. Tsentalovich, N. Fujimura, D. Suzuki, K. P. Soundarapandian, Y. Kawano, M. Pasquali and J. Kono, *Phys. Rev. Materials*, 2018, **2**, 015201.

7 F. Vitale, S. R. Summerson, B. Aazhang, C. Kemere and M. Pasquali, *ACS Nano*, 2015, **9**, 4465–4474.

8 M. McCauley, F. Vitale, C. Young, M. Pasquali and M. Razavi, *Circulation*, 2016, **134**, A20048.

9 M. McCauley, F. Vitale, C. Young, M. Pasquali and M. Razavi, *Circulation*, 2016, **134**, A20132.

10 C. A. Lissandrello, W. F. Gillis, J. Shen, B. W. Pearre, F. Vitale, M. Pasquali, B. J. Holinski, D. J. Chew, A. E. White and T. J. Gardner, *Journal of Neural Engineering*, 2017, **14**, 036006.

11 F. Vitale, D. G. Vercosa, A. V. Rodriguez, S. S. Pamulapati, F. Seibt, E. Lewis, J. S. Yan, K. Badhiwala, M. Adnan, G. Royer-Carfagni, M. Beierlein, C. Kemere, M. Pasquali and J. T. Robinson, *Nano Letters*, 2018, **18**, 326–335.

12 J.-P. Salvetat, G. A. D. Briggs, J.-M. Bonard, R. R. Bacsa, A. J. Kulik, T. Stöckli, N. A. Burnham and L. Forró, *Physical Review Letters*, 1999, **82**, 944–947.

13 L. Zalamea and R. Pipes, *NSTI-Nanotech*, 2006, **1**, 194–197.

14 A. Kis, G. Csayni, J.-P. Salvetat, T.-N. Lee, E. Couteau, A. Kulik, W. Benoit, J. Brugger and L. Forro, *Nature Materials*, 2004, **3**, 153–157.

15 M. Sammalkorpi, A. Krasheninnikov, A. Kuronen, K. Nordlund and K. Kaski, *Nuclear Instruments and Methods in Physics Research B*, 2005, **228**, 142–145.

16 P. Jaroenapibal, D. Luzzi and S. Evoy, *Applied Physics Letters*, 2007, **90**, 081912.

17 R. Pipes, P. Hubert, J.-P. Salvetat and L. Zalamea, *Composites Science and Technology*, 2006, **66**, 1125–1131.

18 R. Pipes and L. Zalamea, *Composites Science and Technology*, 2006, **66**, 2844–2854.

19 B. Yakobson and L. Couchman, *Journal of Nanoparticle Research*, 2006, **8**, 105–110.

20 L. Galuppi and G. Royer-Carfagni, *International Journal of Solids and Structures*, 2012, **49**, 2637–2645.

21 L. Galuppi and G. Royer-Carfagni, *Composites Part B: Engineering*, 2013, **55**, 109–118.

22 M. Bathe, C. Heussinger, M. Claessens, A. Bausch and E. Frey, *Biophysical Journal*, 2008, **94**, 2955–2964.

23 L. Galuppi and G. Royer-Carfagni, *Composites Part B: Engineering*, 2014, **64**, 202–213.

24 W. Morton and J. Hearle, *Physical Properties of Textile Fibres*, Butterworth and Co., London, 1962.

25 S. B. Warner, *Fiber Science*, Prentice Hall, Englewood Cliffs, NJ, 1995.

26 J. C. Guthrie, D. H. Morton and P. H. Oliver, *Journal of the Textile Institute Transactions*, 1954, **45**, T912–T929.

27 T. Mitchell and M. Feughelman, *Textile Research Journal*, 1965, **35**, 311–314.

28 C. F. Zorowski and C. C. S., *Textile Research Journal*, 1965, **35**, 529–538.

29 J. J. Vilatela and A. H. Windle, *Advanced Materials*, 2010, **22**, 4959–4963.

30 J. J. Vilatela and A. H. Windle, *Journal of Engineered Fibers and Fabrics*, 2012, **7**, 23–28.

31 S. Backer, *Textile Research Journal*, 1952, **22**, 668–681.

32 M. M. Platt, W. G. Klein and W. J. Hamburger, *Textile Research Journal*, 1959, **29**, 611–627.

33 D. Tsentalovich, A. Ma, J. Lee, N. Behabtu, E. Bengio, A. Choi, J. Hao, Y. Luo, R. Headrick, M. Green, Y. Talmon and M. Pasquali, *Macromolecules*, 2016, **49**, 681–689.

34 J.-M. Moon, K. An, Y. Lee, Y. Park, D. Bae and G.-S. Park, *Journal of Physical Chemistry B*, 2001, **105**, 5677–5681.

35 T.-J. Park, S. Banerjee, T. Hemraj-Benny and S. Wong, *Journal of Materials Chemistry*, 2006, **16**, 141–154.

36 M. Tran, C. Tridech, A. Alfrey, A. Bismarck and M. Shaffer, *Carbon*, 2016, **45**, 2341–2350.

37 N. Behabtu, C. Young, D. Tsentalovich, O. Kleinerman, X. Wang, A. Ma, E. Bengio, R. ter Waarbeek, J. de Jong, R. Hoogerwerf, S. Fairchild, J. Ferguson, B. Maruyama, J. Kono, Y. Talmon, Y. Cohen, M. Otto and M. Pasquali, *Science*, 2013, **339**, 182–186.

38 D. Tsentalovich, R. J. Headrick, F. Mirri, J. Hao, N. Behabtu, C. C. Young and M. Pasquali, *ACS Applied Materials & Interfaces*, 2017, **9**, 36189–36198.

39 D. Qian, G. J. Wagner, W. K. Liu, M.-F. Yu and R. S. Ruoff, *Applied Mechanics Reviews*, 2002, **55**, 495–533.

40 T. G. Clapp, H. Peng, T. K. Ghosh and J. W. Eischen, *Textile Research Journal*, 1990, **60**, 525–533.

41 C. Brangwynne, G. Koenderink, E. Barry, Z. Dogic, M. MacKintosh and D. Weitz, *Biophysical Journal*, 2007, **93**, 346–359.

42 R. Frisch-Fay, *Flexible Bars*, Butterworths, Washington D.C., 1962.

43 G. Scarpello and D. Ritelli, *International Journal of Mathematics and Mathematical Sciences*, 2011, **2011**, 1–22.

44 F. Hummel and W. Morton, *Philosophical Magazine*, 1927, **4**, 348–357.

45 V. Rohde, *Quarterly of Applied Mathematics*, 1953, **11**, 337–338.

46 K. Sato, *Ingenieur-Archiv*, 1959, **27**, 195–200.

47 H. Denman and R. Schmidt, *Zeitschrift fÃijr angewandte Mathematik und Physik*, 1970, **21**, 412–421.

48 D. DaDeppo and R. Schmidt, *Textile Research Journal*, 1971, **41**, 911–915.

49 Y. Xiao, *Advanced Materials Research*, 2011, **250–253**, 1222–1225.

50 B. Efron, *The Annals of Statistics*, 1979, **7**, 1–26.

51 B. Yakobson, G. Samsonidze and G. Samsonidze, *Carbon*, 2000, **38**, 1675–1680.

52 C. Li, Y. Liu, X. Yao, M. Ito, T. Noguchi and Q. Zheng, *Nanotechnology*, 2010, **21**, 115704.

53 Y. Wang, M. R. Semler, I. Ostanin, E. K. Hobbie and T. Dumitrică, *Materials Today*, 2015, **18**, 265–272.

54 Z. Xu and C. Gao, *Nature Communications*, 2011, **2**, 571.

55 H.-P. Cong, X.-C. Ren and S.-H. Yu, *Scientific Reports*, 2012, **2**, 613.

56 C. Xiang, N. Behabtu, Y. Liu, H. G. Chae, C. C. Young, B. Genorio, D. E. Tsentalovich, C. Zhang, D. V. Kosynkin, J. R. Lomeda, C.-C. Hwang, S. Kumar, M. Pasquali and J. M. Tour, *ACS Nano*, 2013, **7**, 1628–1637.